Published in final edited form as:
Contrast Media Mol Imaging. 2013 ; 8(3): 246–251. doi:10.1002/cmmi.1524.

Simultaneous determination of labile proton fraction ratio and exchange rate with irradiation radio frequency (RF) power dependent quantitative CEST MRI analysis

Phillip Zhe Sun[1,*], **Yu Wang**[1], **Gang Xiao**[2,3,4], and **Renhua Wu**[3,4,*]

[1]Athinoula A. Martinos Center for Biomedical Imaging, Department of Radiology, Massachusetts General Hospital and Harvard Medical School, Charlestown, MA 02129, USA

[2]Department of Math and Applied Mathematics, Hanshan Normal University, Chaozhou, Guangdong, China

[3]Department of Radiology, 2nd Affiliated Hospital of Shantou University Medical College

[4]Provincial Key Laboratory of Medical Molecular Imaging, Shantou, Guangdong, China

Abstract

Chemical exchange saturation transfer (CEST) imaging is sensitive to dilute proteins/peptides and microenvironmental properties, and has been increasingly evaluated for molecular imaging and in vivo applications. However, the experimentally measured CEST effect depends on the CEST agent concentration, exchange rate and relaxation time. In addition, there may be non-negligible direct radio-frequency (RF) saturation effects, particularly severe for diamagnetic CEST (DIACEST) agents due to their relatively small chemical shift difference from that of the bulk water resonance. As such, the commonly used asymmetry analysis only provides CEST-weighted information. Recently, it has been shown with numerical simulation that both labile proton concentration and exchange rate can be determined by evaluating the RF power dependence of DIACEST effect. To validate the simulation results, we prepared and imaged two CEST phantoms: a pH phantom of serially titrated pH at a fixed creatine concentration and a concentration phantom of serially varied creatine concentration titrated to the same pH, and solved the labile proton fraction ratio and exchange rate per-pixel. For the concentration phantom, we showed that the labile proton fraction ratio is proportional to the CEST agent concentration with negligible change in the exchange rate. Additionally, we found the exchange rate of the pH phantom is dominantly base-catalyzed with little difference in the labile proton fraction ratio. In summary, our study demonstrated quantitative DIACEST MRI, which remains promising to augment the conventional CEST-weighted MRI analysis.

Keywords

amide proton transfer (APT); chemical exchange saturation transfer (CEST); pH

[*]**Correspondence Authors:** Dr. Phillip Zhe Sun (pzhesun@nmr.mgh.harvard.edu) Martinos Center, MGH and Harvard Medical School Rm 2301, 149 13th Street, Charlestown, MA 02129, USA Tel: 617-726-4060, Fax: 617-726-7422 or Dr. Renhua Wu (rhwu@stu.edu.cn) 2nd Affiliated Hospital of Shantou University Medical College Shantou 515041, Guangdong, China Tel: (86) 0754-88915674.

1. INTRODUCTION

Chemical exchange saturation transfer (CEST) MRI is sensitive to dilute CEST agents and microenvironmental properties, and remains promising for molecular imaging and in vivo applications (1-10). For instance, amide proton transfer (APT) MRI, a variant of CEST MRI, has been applied to study diseases such as acute stroke, cancer and multiple sclerosis (11-19). However, the commonly used CEST MRI analysis provides very crude information about the underlying CEST system. Specifically, the CEST effect is sensitive to both the labile proton ratio and exchange rate, and strongly depends on the experimental conditions (20-23). As such, it is challenging to determine the CEST agent concentration and exchange rate simultaneously, and simplification has to be made. For instance, in the case of APT imaging of acute stroke, the apparent APT MRI contrast has been attributed to tissue acidosis, while assuming negligible change in the endogenous amide proton content (19,24). On the other hand, the APT contrast of cancerous tissue has been postulated to be dominated by mobile proteins/peptides content change with negligible tissue pH variation (25). Whereas such assumptions are likely to be valid as first order approximations, it will be very useful to develop quantitative CEST MRI analysis to simultaneously determine the labile proton ratio and exchange rate, which may better elucidate changes in the underlying CEST system, and ultimately advance the field of quantitative CEST MRI.

Mathematical models, both empirical solutions and numerical simulations, have been developed to describe the CEST effect, often calculated from the asymmetry analysis (26-29). Notably, CEST effect strongly depends on the RF irradiation power (30,31). While higher RF power level is more efficient in saturating labile protons, it also induces non-negligible direct RF saturation (spillover) effect. The RF spillover effect could be particularly severe for diamagnetic CEST (DIACEST) agents due to their relatively small chemical shift difference from that of the bulk water. Therefore, for DIACEST agents undergoing slow and intermediate chemical exchange, the CEST effect initially increases with RF power but plateaus and subsequently decreases when RF power becomes too high. Indeed, it has been shown with numerical simulation that the optimal RF power level strongly depends on the chemical exchange rate but not the labile proton concentration (32). It suggests that although different combinations of labile proton concentration and exchange rate may yield approximately the same CEST effect for a given RF power level, it is possible to differentiate their independent contribution by probing the RF power dependence of CEST (RFP-CEST) MRI. To test this, we engineered two DIACEST phantoms: a pH phantom with serially titrated pH at the same creatine concentration and a concentration phantom of serially varied creatine concentration at identical pH. We acquired CEST MRI under multiple RF power levels, and estimated the labile proton fraction ratio and exchange rate using an empirical solution that takes experimental factors (i.e. labeling coefficient and spillover factor) into account (30). The derived labile proton fraction ratio and exchange rate were in good agreement with the phantom properties. In summary, our study demonstrated quantitative DIACEST MRI, which remains promising to augment the conventional CEST-weighted MRI analysis.

2. RESULTS

We obtained CEST MRI from both pH and concentration phantoms under different RF irradiation levels. For the pH phantom, creatine concentration was 60 mM while their pH was serially varied from 5.99 to 7.24. Fig. 1 a shows CEST images obtained under three representative RF power levels, 0.5, 0.8 and 1.8 μT. Notably, at weak RF irradiation (i.e. 0.5 μT), CEST effect for pH compartments of 6.48 and 6.75 was slightly stronger than that of higher pH compartments. The CEST effect increased for B_1 of 0.8 μT and was approximately the same for pH compartments of 6.75, 7.02 and 7.24. The CEST effect further increased when B_1 was 1.8 μT, with the compartment of pH 7.24 showing the highest CEST effect. For the concentration phantom, the creatine concentration was serially varied from 20 to 100 mM while their pH was titrated to 6.75 (Fig. 1 b). Interestingly, CEST effect increased consistently with creatine concentration for all three RF amplitudes. This is different from that of the pH phantom, where the maximum CEST effect of the highest pH was not achieved until higher RF amplitude was used. This is because the saturation efficiency strongly varies with the ratio of the RF irradiation amplitude and exchange rate, less dependent on the labile proton concentration (32,33). Because the creatine amine proton exchange is dominantly base-catalyzed, it takes relatively strong RF irradiation to saturate labile protons undergoing faster chemical exchange at higher pH. While on the other hand, the exchange rate was the same for the concentration phantom, and CEST effect simply scaled with creatine concentration.

We measured phantom T_1 and T_2 (Fig. 2). For the pH phantom, R_{1w} showed very little change with pH, which can be described by linear regression $-0.000726*pH + 0.335\ s^{-1}$ (R^2=0.156, P>0.50). R_{2w} increased exponentially with pH, suggesting base-catalyzed amine proton chemical exchange (R^2=0.972, P=0.01). For the concentration phantom, both R_{1w} and R_{2w} can be described by linear regression, with $R_{1w}=9.52*10^{-5}*f + 0.332$ (R^2=0.918, P=0.01) and $R_{2w}=0.00377*f + 0.499$ (R^2=0.938, P<0.01), where f is creatine concentration in mM. Note that the change of R_{2w} with pH and creatine concentration was significantly stronger than that of R_{1w}, consistent with the findings of Aime et al. (34) In addition, the bulk water T_{1w} and T_{2w} can be obtained by extrapolating the relaxation measurements with respect to the creatine concentration, being 3.0 s and 2.0 s, respectively.

The empirical solution can describe B_1-dependent CEST effect for both pH and concentration phantoms. For the pH phantom, the CEST effect initially increased with RF amplitude but peaked and subsequently decreased for higher RF amplitudes (Fig. 3 a). The fitting agreed well with the experimental measurements (R^2=0.998). In addition, Fig. 3 b shows that the optimal RF amplitude significantly increased with pH (R^2=0.992, P=0.03). The empirical solution can also describe the B_1 dependence of CEST measurements from the concentration phantom (R^2=0.998, Fig. 3 c). Notably, Fig. 3 d shows that the optimal RF amplitude had little dependence on the CEST agent concentration (R^2=0.762, P>0.05). This suggests that the optimal RF irradiation level depends on the exchange rate but not the labile proton ratio, consistent with findings obtained from numerical simulation (32).

Fig. 4 shows the numerically derived labile proton ratio and exchange rate maps. For the pH phantom, the labile proton fraction ratio (Fig. 4a) had very little change while the exchange

rate (Fig. 4b) increased exponentially with pH. For the concentration phantom, the labile proton ratio (Fig. 4c) increased significantly with the creatine concentration while there was very little change in the exchange rate (Fig. 4 d). The pixel-wise fitting took approximately 5 s using a Dell Precision T7400 desktop computer. The labile proton ratio and exchange rate were evaluated as functions of pH and creatine concentration (Fig. 5). For the pH phantom, the labile proton fraction ratio was $0.00142 \pm 1.53\times10^{-4}$ (mean ±S.D.) with little change with pH (R^2=0.603, P>0.12). The exchange rate can be described by a base-catalyzed exchange relationship, (i.e., $k_{sw}=0.0435+ 0.189*10^{(pH-3.764)}$, R^2=0.996, P<0.03). For the concentration phantom, the labile proton fraction ratio was $f_r=2.04*10^{-5}*f + 1.22*10^{-4}$ (R^2=0.994, P<0.01). Notably, the intercept was not significantly different from 0 (P>0.12), suggesting good linear relationship between the numerically derived labile proton ratio and creatine concentration. In addition, the exchange rate showed very little variation with creatine concentration, being $169 \pm 18\ s^{-1}$ (R^2=0.0903, P>0.60). It is important to point out that the fitting results were in good agreement, despite that phantoms were measured separately. The labile proton fraction ratio from the concentration phantom of 60 mM was $0.00131 \pm 8.54\times 10^{-5}$, in agreement with that of the pH phantom (i.e. $0.00142\pm1.53\times10^{-4}$). In addition, the exchange rate for the pH compartment of 6.75 was $177\pm13\ s^{-1}$, in excellent agreement with the exchange rate derived from the concentration phantom, being $169\pm18\ s^{-1}$.

3. DISCUSSION

Our study demonstrated that RF power-dependent DIACEST MRI analysis is capable of simultaneously determining the labile proton fraction ratio and exchange rate, augmenting the conventional CEST-weighted image analysis. Indeed, there is an unmet biomedical need of delineating pH/exchange rate from the contrast agent concentration, particularly useful for quantitative molecular imaging. Notably, Dixon et al. demonstrated that for paramagnetic CEST (PARACEST) agents, the chemical exchange rate can be determined independent of the CEST agent concentration, and dubbed it omega plot (35). Whereas it provides accurate quantification of PARACEST agents due to their large chemical shift from the bulk water resonance and hence negligible concomitant RF spillover effects, the use of omega plot is somewhat limited for DIACEST agents because of their relatively small chemical shift. This is because without correction of RF spillover effects, the omega-plot analysis treats direct RF saturation as the CEST effect, resulting in gross overestimation of labile proton ratio and exchange rate. As such, our study complements the omega plot analysis for quantifying DIACEST MRI. In addition, ratiometric CEST MRI has been proposed to normalize the CEST agent concentration factor for solving chemical exchange rate (9,36,37). However, it only applies to CEST agents with multiple chemically distinguishable labile protons, which the proposed qCEST analysis here does not require.

The effect of RF irradiation power upon CEST measurement has been increasingly recognized. Whereas the RF spillover effect has often been considered as an adverse effect, we showed that the RF power dependence of CEST MRI might serve as a useful parameter for improved quantification of the underlying CEST system. Specifically, the RF labeling coefficient depends on the ratio of RF irradiation amplitude and exchange rate. Therefore, when weak B_1 field is used, the saturation coefficient is higher for slower chemical

exchange and hence stronger CEST effect than that from faster chemical exchange rate. While on the other hand, for strong B_1 field, the saturation efficiency continues to increase for faster chemical exchange rate while it plateaus for slower chemical exchange rate. Hence, the CEST effect continues to increase for faster chemical exchange rate while that of the slower exchange peaks and subsequently decreases due to increasing direct RF saturation at high B_1 irradiation level. As such, it is necessary to include both weak and strong RF power levels when quantifying the underlying CEST system. Whereas we used fourteen B_1 levels in our analysis, we found that the labile proton ratio and exchange rate can be reasonably estimated with three or four B_1 levels, provided that both weak and strong RF levels were included. It is important to note that numerical simulation shows that qCEST MRI analysis requires precise measurement of T_{1w} and T_{2w} (32). This is because RF spillover effect decreases at long T_{2w}. Therefore, if T_{2w} is overestimated, the spillover factor will be under-corrected, resulting in an underestimated exchange rate and overestimated labile proton ratio. On the other hand, T_{1w} relaxation competes with saturation transfer, and for the same exchange rate, less B_1 field is needed for higher T_{1w}. Therefore, if T_{1w} is overestimated, the exchange rate will be overestimated and the labile proton ratio underestimated. In addition, when long RF irradiation is used, the effects of labile proton T_1 and T_2 (i.e. T_{1s} and T_{2s}) upon the numerical solution were minimal. Nevertheless, our study demonstrated that accurate relaxation measurement could be obtained with well-established experimental protocols.

We also analyzed the precision of the proposed qCEST MRI analysis. The coefficient of variance was calculated using the labile proton ratio estimated from the pH phantom (i.e. $0.00142 \pm 1.53\times10^{-4}$) and the chemical exchange rate derived from the concentration phantom (i.e. $169 \pm 18\ s^{-1}$), both being about 11%. Whereas field homogeneity was reasonably good in our system and no field correction was necessary, the measurement might benefit from rigorous field correction approaches (38,39). However, this may significantly prolong the scan time, as images at multiple offsets have to be acquired for each RF power level, which is beyond the scope of our current work. This may be partially addressed with the ongoing development of sensitive and optimized CEST acquisition strategies (40-43). It is necessary to point out that further study is needed to evaluate whether the proposed approach can be extended to characterize CEST systems containing multiple exchangeable sites (27,28). For instance, in addition to amide proton exchange, the endogenous APT MRI may be susceptible to CEST effect from amine and hydroxyl groups (10,24). In addition, there are concomitant macromolecular magnetization transfer (MT) effects in vivo (44,45). Recent data have suggested that the MT contribution may be reasonably compensated by Lorentzian fitting and/or chemical exchange rotation transfer (CERT) MRI, which will be evaluated in our future work (46,47). Nevertheless, to the best of our knowledge, our study here is the first to demonstrate simultaneous pixel-wise mapping of labile proton ratio and exchange rate from DIACEST MRI, complementing the conventional CEST-weighted analysis.

4. CONCLUSIONS

Our study demonstrated that both the labile proton fraction ratio and exchange rate maps could be simultaneously determined from analyzing the RF power dependence of DIACEST

MRI measurement. Therefore, quantitative CEST analysis is feasible and remains promising to augment the commonly used yet oversimplified DIACEST MRI analysis for improved definition of the underlying CEST system.

5. METHODS

PHANTOM

CEST phantoms were prepared with creatine and phosphate buffer solution (PBS, Sigma Aldrich, St Louis, MO), as described previously (48). For the pH phantom, pH was serially titrated to 5.99, 6.48, 6.75, 7.02 and 7.24 (EuTech Instrument, Singapore), while the creatine concentration was fixed to 60 mM. For the concentration phantom, we serially diluted the creatine concentration from 100, 80, 60, 40 to 20 mM, and titrated their pH to 6.75 within 0.01. The solution was transferred into centrifuge tubes, sealed and inserted into two phantom containers. The containers were then filled with 1% low gelling point agarose solution to fixate the creatine-PBS tubes.

MRI

Phantoms were imaged separately at 4.7 Tesla with a standard volume RF resonator (Bruker Biospec, Billerica, MA) under the room temperature of approximately 20°C. Images were obtained with single-shot echo planar imaging (EPI). We chose a slice thickness of 5 mm, field of view (FOV) of 76 × 76 mm and imaging matrix of 64 × 64 with an EPI acquisition bandwidth of 200 kHz. We acquired 3-point CEST imaging with continuous wave (CW) RF irradiation applied at ±1.875 ppm (± 375 Hz at 4.7 Tesla), in addition to a control scan without RF irradiation (repetition time (TR)/echo time (TE)=22,000/28 ms, time of saturation (TS) =10,000 ms, number of average (NSA)=2). CEST effect was calculated from CEST ratio (CESTR), being $(I_{ref} - I_{label})/I_0$, where I_{ref} and I_{label} are the reference and label scans, respectively, and I_0 is the control scan. The RF power level was systematically varied from 0.3 to 3 μT: from 0.3 to 1 μT with an increment step of 0.1 μT, followed by 1.25, 1.5, 1.75, 2, 2.5 and 3 μT. In addition, T_1-weighted images were acquired using an inversion recovery sequence with eight inversion intervals (TI) from 250 to 10,000 ms (recovery time/TE =12,000/28 ms, NAE=2). T_2 map was derived from five separate spin echo images with TE ranging from 50 to 500 ms (TR=12,000 ms, NSA=2)(49). The B_0 map was obtained by acquiring four asymmetrical spin echo (ASE) phase images with off-centered echo time being 1, 3, 5 and 7 ms (TR/TE=12,000/36 ms, NSA=2). The B_1 field was calibrated by varying the pre-pulse flip angle (θ) from 10° to 180°, with intervals of 10° (TR/TE=12,000/28 ms, NSA=2).

Data Processing—Data were processed in Matlab (Matheworks, Natick, MA). The CEST effect was described using the empirical solution (30):

$$\mathrm{CESTR}=\frac{\mathrm{f_r}\cdot \mathrm{k}_{sw}}{\mathrm{R}_{1w}+\mathrm{f_r}\cdot \mathrm{k}_{sw}}\cdot\alpha\cdot(1-\sigma) \quad (1)$$

where α is the labeling coefficient, σ is the spillover factor, k_{sw} is the chemical exchange rate from labile protons to bulk water, f_r is labile proton fraction ratio with respect to bulk water proton, and R_{1w} is bulk water longitudinal relaxation rate (20,31). The labeling

coefficient is given by $\frac{(2\pi\gamma B_1)^2}{p \cdot q+(2\pi\gamma B_1)^2}$, where B_1 is the irradiation RF amplitude and γ is the gyromagnetic ratio, $p=r_{2s}-\frac{k_{sw}k_{ws}}{r_{2w}}$ and $q=r_{1s}-\frac{k_{sw}k_{ws}}{r_{1w}}$, in which $k_{ws} = f_r \cdot k_{sw}$ (20). Moreover, $r_{1w,s}=R_{1,ws}+k_{ws,sw}$ and $r_{2w,s}=R_{2w,s}+k_{ws,sw}$, respectively. In addition, the spillover factor is equal to

$$1-\frac{r_{1w}}{k_{ws}}\left(\frac{R_{1w}r_{zs}cos^2\theta+R_{1s}k_{ws}\,cos\,\theta\,cos^2\,(\theta/2)}{r_{zw}r_{zs}-k_{ws}k_{sw}cos^2\,(\theta/2)}-\frac{R_{1w}r_{2s}\,cos^2\,\theta}{r_{zw}r_{2s}-k_{ws}k_{sw}\,sin^2\,\theta}\right),$$

where $r_{zw} = r_{1w}\cos^2\theta/2+r_{2w}\sin^2\theta/2$, $r_{zs} = r_{1s}\cos^2\theta+r_{2s}\sin^2\theta$, $\theta = \tan^{-1}(2\pi\gamma B_1/\Delta\omega_s)$ and $\Delta\omega_s$ is the labile proton chemical shift (50). For the numerical fitting, T_{1w} and T_{2w} were derived from extrapolation of the experimental measurements as a function of creatine concentration, found to be 3.0 s and 2.0 s, respectively. In addition, we assumed T_{1s} and T_{2s} to be 1.0 s and 15 ms. Two free parameters (i.e. labile proton fraction ratio and exchange rate) were obtained pixel-wise from the least squares fitting of the empirical solution (Eq. 1). To minimize the bias of the initial guess, we chose identical initial guesses of labile proton fraction ratio and exchange rate for all pixels, being 1:1000 and 200 s^{-1}, respectively. In addition, the lower and upper limits for labile proton fraction ratio were 1:2500 and 1:250 while the lower and upper limits for the exchange rates were 10 and 1000 s^{-1}, respectively. The maximal number of iteration was set to be 10,000 times. The pixel-wise fitting took approximately 5 min for each phantom using a Dell Precision T7400 desktop computer. Moreover, the B_0 map was derived by linearly fitting the obtained phase map (φ) against the off-centered echo time ($\Delta\tau$) using $B_0=\frac{2\pi}{\gamma}\frac{\varphi}{\Delta\tau}$. The magnetic field was reasonably homogeneous, with B_0 field map being 5 ± 5 Hz and 2 ± 4 Hz for the pH and concentration phantoms, respectively. B_1 field was solved by fitting the image intensity using $I(\theta) = I_0 \cdot |\cos\gamma \cdot (\eta \cdot B_1 + \Delta B_1) \cdot \tau|$, where η and ΔB_1 are the scaling factor and offset of the B_1 field, respectively, and θ is the flip angle. We found $\Delta B_1 = -0.21$ and $\eta = 1.02$. The calibrated RF power level was 0.1, 0.2, 0.3, 0.4, 0.5, 0.6, 0.7, 0.8, 1.0, 1.3, 1.5, 1.8, 2.3 and 2.7 μT. The B_1 inhomogeneity for the volume RF coil has been found to be within 5 %. Because both B_0 and B_1 fields were reasonably homogeneous, no field correction for CEST MRI was necessary (38,39).

Acknowledgments

This study was supported in part by grants from AHA/SDG 0835384N, NIH/NIBIB 1K01EB009771, NIH/NCRR-P41RR14075 and NSFC 30930027.

REFERENCES

1. Forsen S, Hoffman RA. Study of moderately rapid chemical exchange reactions by means of nuclear magnetic double resonance. J Chem Phys. 1963; 39:2892–2901.
2. Ward KM, Aletras AH, Balaban RS. A new class of contrast agents for MRI based on proton chemical exchange dependent saturation transfer (CEST). J Magn Reson. 2000; 143:79–87. [PubMed: 10698648]
3. Aime S, Delli CD, Terreno E. Highly sensitive MRI chemical exchange saturation transfer agents using liposomes. Angew Chem Int Ed Engl. 2005; 44(34):5513–5515. [PubMed: 16052647]

4. Zhang S, Malloy CR, Sherry AD. MRI Thermometry Based on PARACEST Agents. J Am Chem Soc. 2005; 127(50):17572–17573. [PubMed: 16351064]
5. Gilad AA, McMahon MT, Walczak P, Winnard PT Jr. Raman V, van Laarhoven HW, Skoglund CM, Bulte JW, van Zijl PC. Artificial reporter gene providing MRI contrast based on proton exchange. Nat Biotechnol. 2007; 25(2):217–219. [PubMed: 17259977]
6. Yoo B, Raam MS, Rosenblum RM, Pagel MD. Enzyme-responsive PARACEST MRI contrast agents: a new biomedical imaging approach for studies of the proteasome. Contrast Media Mol Imaging. 2007; 2(4):189–198. [PubMed: 17712869]
7. van Zijl PCM, Yadav NN. Chemical exchange saturation transfer (CEST): What is in a name and what isn't? Magn Reson Med. 2011; 65(4):927–948. [PubMed: 21337419]
8. Hancu I, Dixon WT, Woods M, Vinogradov E, Sherry AD, Lenkinski RE. CEST and PARACEST MR contrast agents. Acta Radiologica. 2010; 51(8):910–923. [PubMed: 20828299]
9. Li Y, Sheth VR, Liu G, Pagel MD. A self-calibrating PARACEST MRI contrast agent that detects esterase enzyme activity. Contrast Media Mol Imaging. 2011; 6(4):219–228. [PubMed: 21861282]
10. Cai K, Haris M, Singh A, Kogan F, Greenberg JH, Hariharan H, Detre JA, Reddy R. Magnetic resonance imaging of glutamate. Nat Med. 2012; 18(2):302–306. [PubMed: 22270722]
11. Zhou J, Payen JF, Wilson DA, Traystman RJ, van Zijl PC. Using the amide proton signals of intracellular proteins and peptides to detect pH effects in MRI. Nat Med. 2003; 9(8):1085–1090. [PubMed: 12872167]
12. Sun PZ, Zhou J, Sun W, Huang J, van Zijl PC. Detection of the ischemic penumbra using pH-weighted MRI. J Cereb Blood Flow Metab. 2007; 27(6):1129–1136. [PubMed: 17133226]
13. Jokivarsi KT, Gröhn HI, Gröhn OH, Kauppinen RA. Proton transfer ratio, lactate, and intracellular pH in acute cerebral ischemia. Magn Reson Med. 2007; 57(4):647–653. [PubMed: 17390356]
14. Mougin OE, Coxon RC, Pitiot A, Gowland PA. Magnetization transfer phenomenon in the human brain at 7 T. NeuroImage. 2010; 49(1):272–281. [PubMed: 19683581]
15. Sun PZ, Cheung JS, Wang EF, Lo EH. Association between pH-weighted endogenous amide proton chemical exchange saturation transfer MRI and tissue lactic acidosis during acute ischemic stroke. J Cereb Blood Flow Metab. 2011; 31(8):1743–1750. [PubMed: 21386856]
16. Shah T, Lu L, Dell KM, Pagel MD, Griswold MA, Flask CA. CEST-FISP: A novel technique for rapid chemical exchange saturation transfer MRI at 7 T. Magn Reson Med. 2011; 65(2):432–437. [PubMed: 20939092]
17. Dula AN, Asche EM, Landman BA, Welch EB, Pawate S, Sriram S, Gore JC, Smith SA. Development of chemical exchange saturation transfer at 7T. Magn Reson Med. 2012; 66(3):831–838. [PubMed: 21432902]
18. Jia G, Abaza R, Williams JD, Zynger DL, Zhou J, Shah ZK, Patel M, Sammet S, Wei L, Bahnson RR, Knopp MV. Amide proton transfer MR imaging of prostate cancer: A preliminary study. J Magn Reson Imag. 2011; 33(3):647–654.
19. Sun PZ, Wang EF, Cheung JS. Imaging acute ischemic tissue acidosis with pH-sensitive endogenous amide proton transfer (APT) MRI – Correction of tissue relaxation and concomitant RF irradiation effects toward mapping quantitative cerebral tissue pH. Neuroimage. 2012; 60(1): 1–6. [PubMed: 22178815]
20. Zhou J, Wilson DA, Sun PZ, Klaus JA, van Zijl PCM. Quantitative description of proton exchange processes between water and endogenous and exogenous agents for WEX, CEST, and APT experiments. Magn Reson Med. 2004; 51:945–952. [PubMed: 15122676]
21. McMahon M, Gilad A, Zhou J, Sun PZ, Bulte J, van Zijl PC. Quantifying exchange rates in chemical exchange saturation transfer agents using the saturation time and saturation power dependencies of the magnetization transfer effect on the magnetic resonance imaging signal (QUEST and QUESP): Ph calibration for poly-L-lysine and a starburst dendrimer. Magn Reson Med. 2006; 55(4):836–847. [PubMed: 16506187]
22. Wu R, Liu C, Liu P, Sun PZ. Improved measurement of labile proton concentration-weighted chemical exchange rate (kws) with experimental factor-compensated and T1-normalized quantitative chemical exchange saturation transfer (CEST) MRI. Contrast Media & Molecular Imaging. 2012; 7(4):384–389. [PubMed: 22649044]

23. Sun PZ. Simplified quantification of labile proton concentration-weighted chemical exchange rate (kws) with RF saturation time dependent ratiometric analysis (QUESTRA): Normalization of relaxation and RF irradiation spillover effects for improved quantitative chemical exchange saturation transfer (CEST) MRI. Magn Reson Med. 2012; 67(4):936–942. [PubMed: 21842497]
24. Jin T, Wang P, Zong X, Kim S-G. Magnetic resonance imaging of the Amine Proton EXchange (APEX) dependent contrast. NeuroImage. 2012; 16(2):1218–1227. [PubMed: 21871570]
25. Salhotra A, Lal B, Laterra J, Sun PZ, van Zijl PCM, Zhou J. Amide proton transfer imaging of 9L gliosarcoma and human glioblastoma xenografts. NMR Biomed. 2008; 21:489–497. [PubMed: 17924591]
26. Woessner DE, Zhang S, Merritt ME, Sherry AD. Numerical solution of the Bloch equations provides insights into the optimum design of PARACEST agents for MRI. Magn Reson Med. 2005; 53(4):790–799. [PubMed: 15799055]
27. Li AX, Hudson RHE, Barrett JW, Johns CK, Pasternak SH, Bartha R. Four-pool modeling of proton exchange processes in biological systems in the presence of MRI-paramagnetic chemical exchange saturation transfer (PARACEST) agents. Magn Reson Med. 2008; 60(5):1197–1206. [PubMed: 18958857]
28. Sun PZ. Simplified and scalable numerical solution for describing multi-pool chemical exchange saturation transfer (CEST) MRI contrast. J Magn Reson. 2010; 205(2):235–241. [PubMed: 20570196]
29. Murase K, Tanki N. Numerical solutions to the time-dependent Bloch equations revisited. Magn Reson Imaging. 2011; 29(1):126–131. [PubMed: 20832224]
30. Sun PZ, van Zijl PCM, Zhou J. Optimization of the irradiation power in chemical exchange dependent saturation transfer experiments. J Magn Reson. 2005; 175(2):193–200. [PubMed: 15893487]
31. Sun PZ, Zhou J, Huang J, van Zijl P. Simplified quantitative description of amide proton transfer (APT) imaging during acute ischemia. Magn Reson Med. 2007; 57(2):405–410. [PubMed: 17260362]
32. Sun PZ. Simultaneous determination of labile proton concentration and exchange rate utilizing optimal RF power: radio frequency power (RFP) dependence of chemical exchange saturation transfer (CEST) MRI. J Magn Reson. 2010; 202(2):155–161. [PubMed: 19926319]
33. Aime S, Calabi L, Biondi L, Miranda MD, Ghelli S, Paleari L, Rebaudengo C, Terreno E. Iopamidol: Exploring the potential use of a well-established x-ray contrast agent for MRI. Magn Reson Med. 2005; 53(4):830–834. [PubMed: 15799043]
34. Aime S, Fedeli F, Sanino A, Terreno E. A R2/R1 Ratiometric Procedure for a Concentration-Independent, pH-Responsive, Gd(III)-Based MRI Agent. J Am Chem Soc. 2006; 128(35):11326–11327. [PubMed: 16939235]
35. Dixon TW, Ren J, Lubag A, J. M, Ratnakar J, Vinogradov E, Hancu I, Lenkinski R, E. Sherry AD. A concentration-independent method to measure exchange rates in PARACEST agents. Magn Reson Med. 2010; 63(3):625–632. [PubMed: 20187174]
36. Ward KM, Balaban RS. Determination of pH using water protons and chemical exchange dependent saturation transfer (CEST). Magn Reson Med. 2000; 44:799–802. [PubMed: 11064415]
37. Longo DL, Dastrù W, Digilio G, Keupp J, Langereis S, Lanzardo S, Prestigio S, Steinbach O, Terreno E, Uggeri F, Aime S. Iopamidol as a responsive MRI-chemical exchange saturation transfer contrast agent for pH mapping of kidneys: In vivo studies in mice at 7 T. Magn Reson Med. 2011; 65(1):202–211. [PubMed: 20949634]
38. Kim M, Gillen J, Landman BA, Zhou J, van Zijl PCM. Water saturation shift referencing (WASSR) for chemical exchange saturation transfer (CEST) experiments. Magn Reson Med. 2009; 61(6):1441–1450. [PubMed: 19358232]
39. Sun PZ, Farrar CT, Sorensen AG. Correction for artifacts induced by B0 and B1 field inhomogeneities in pH-sensitive chemical exchange saturation transfer (CEST) imaging. Magn Reson Med. 2007; 58(6):1207–1215. [PubMed: 17969015]
40. Sun PZ, Benner T, Kumar A, Sorensen AG. Investigation of optimizing and translating pH-sensitive pulsed-chemical exchange saturation transfer (CEST) imaging to a 3T clinical scanner. Magn Reson Med. 2008; 60(4):834–841. [PubMed: 18816867]

41. Sun PZ, Wang EF, Cheung JS, Zhang XA, Benner T, Sorensen AG. Simulation and optimization of pulsed radio frequency (RF) irradiation scheme for chemical exchange saturation transfer (CEST) MRI – demonstration of pH-weighted pulsed-amide proton CEST MRI in an animal model of acute cerebral ischemia. Magn Reson Med. 2011; 66(4):1042–1048. [PubMed: 21437977]
42. Zu Z, Li K, Janve VA, Does MD, Gochberg DF. Optimizing pulsed-chemical exchange saturation transfer imaging sequences. Magn Reson Med. 2011; 66(4):1100–1108. [PubMed: 21432903]
43. Sun PZ, Cheung JS, Wang E, Benner T, Sorensen AG. Fast multi-slice pH-weighted chemical exchange saturation transfer (CEST) MRI with unevenly segmented RF irradiation. Magn Reson Med. 2011; 65(2):588–594. [PubMed: 20872859]
44. Hua J, Jones CK, Blakeley J, Smith SA, van Zijl PCM, Zhou J. Quantitative description of the asymmetry in magnetization transfer effects around the water resonance in the human brain. Magn Reson Med. 2007; 58(4):786–793. [PubMed: 17899597]
45. Ling W, Regatte RR, Navon G, Jerschow A. Assessment of glycosaminoglycan concentration in vivo by chemical exchange-dependent saturation transfer (gagCEST). Proc Natl Acad Sci. 2008; 105(7):2266–2270. [PubMed: 18268341]
46. Zaiβ M, Schmitt B, Bachert P. Quantitative separation of CEST effect from magnetization transfer and spillover effects by Lorentzian-line-fit analysis of z-spectra. J Magn Reson. 2011; 211(2):149–155. [PubMed: 21641247]
47. Zu Z, Janve VA, Xu J, Does MD, Gore JC, Gochberg DF. A new method for detecting exchanging amide protons using chemical exchange rotation transfer. Magn Reson Med. 2012 in press.
48. Sun PZ, Sorensen AG. Imaging pH using the chemical exchange saturation transfer (CEST) MRI: correction of concomitant RF irradiation effects to quantify CEST MRI for chemical exchange rate and pH. Magn Reson Med. 2008; 60(2):390–397. [PubMed: 18666128]
49. Cheung JS, Wang EF, Zhang XA, Manderville E, Lo EH, Sorensen AG, Sun PZ. Fast radio-frequency enforced steady state (FRESS) spin echo MRI for quantitative T2 mapping: minimizing the apparent repetition time (TR) dependence for fast T2 measurement. NMR Biomed. 2012; 25(2):189–194. [PubMed: 21755552]
50. Baguet E, Roby C. Off-resonance irradiation effect in steady-state NMR saturation transfer. J Magn Reson. 1997; 128(2):149–160. [PubMed: 9356270]

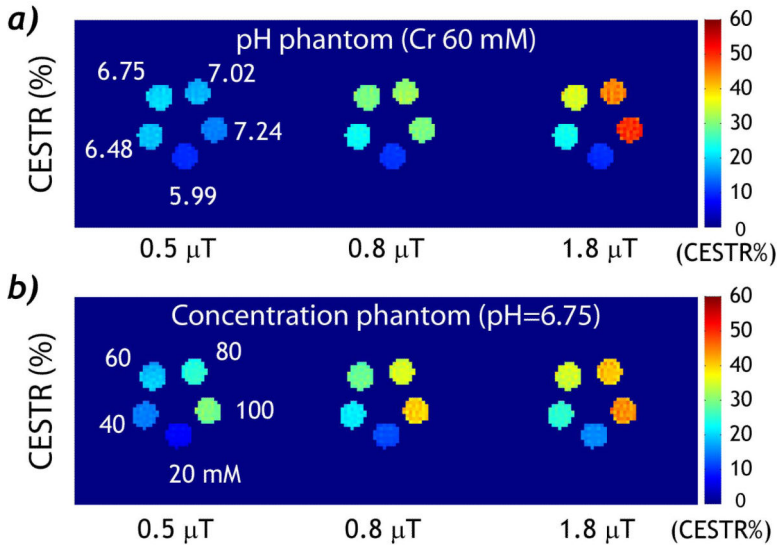

Fig. 1.

RF power level-dependent CEST images. a) CEST images calculated from the asymmetry analysis show that the CEST effect for each pH sample increases with RF power (Cr= 60 mM). b) CEST effect increases with creatine concentration and RF power (pH= 6.75).

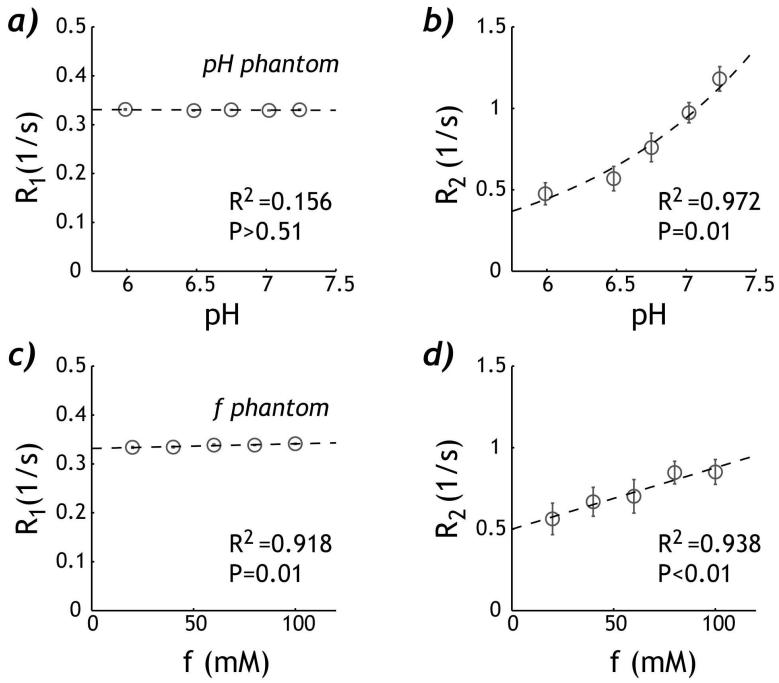

Fig. 2.

Relaxation measurements of the pH and concentration DIACEST phantoms. a) R_{1w} for the pH phantom shows very little change with pH. b) R_{2w} for the pH phantom increases exponentially with pH, suggesting base-catalyzed chemical exchange. c) R_{1w} for the concentration phantom shows very little yet significant change with the creatine concentration. d) R_{2w} of the concentration phantom increases approximately linearly with creatine concentration.

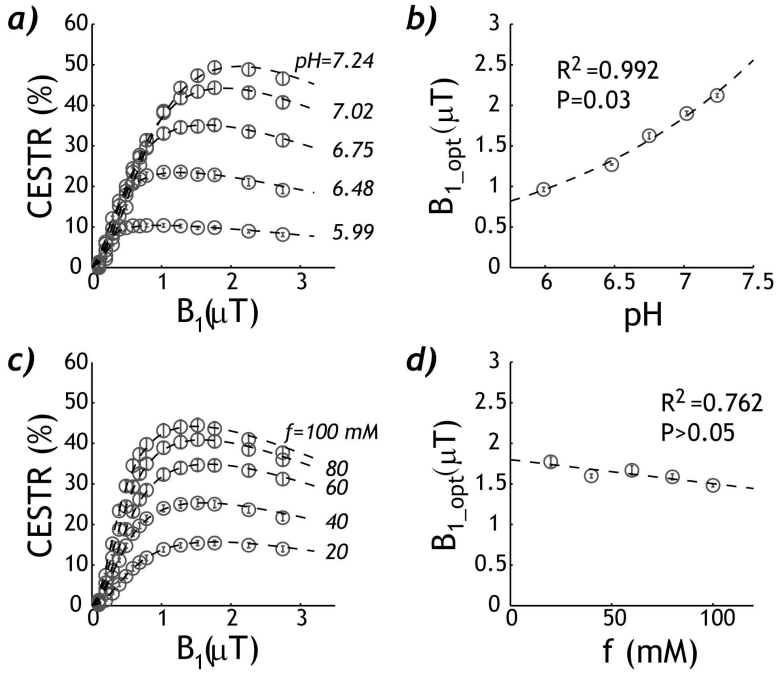

Fig. 3.

Description of RF power level-dependent CEST effect. a) The empirical solution describes the RF power dependent CEST effect of the pH phantom. b) The optimal RF power level increases with pH. c) The RF power dependence of CEST effect of the concentration phantom can also be described by the empirical solution. d) The optimal RF power level shows little change with the creatine concentration.

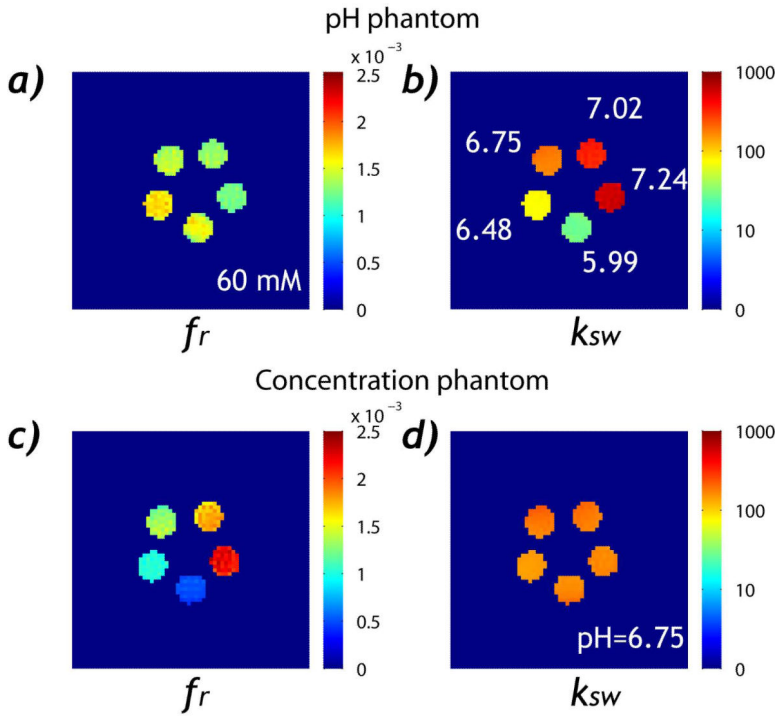

Fig. 4.

Mapping the labile proton fraction ratio and exchange rate. a) The labile amine proton fraction ratio map for the pH phantom. b) The exchange rate map for the pH phantom. c) The labile proton ratio map for the concentration phantom. d) The exchange rate map for the concentration phantom.

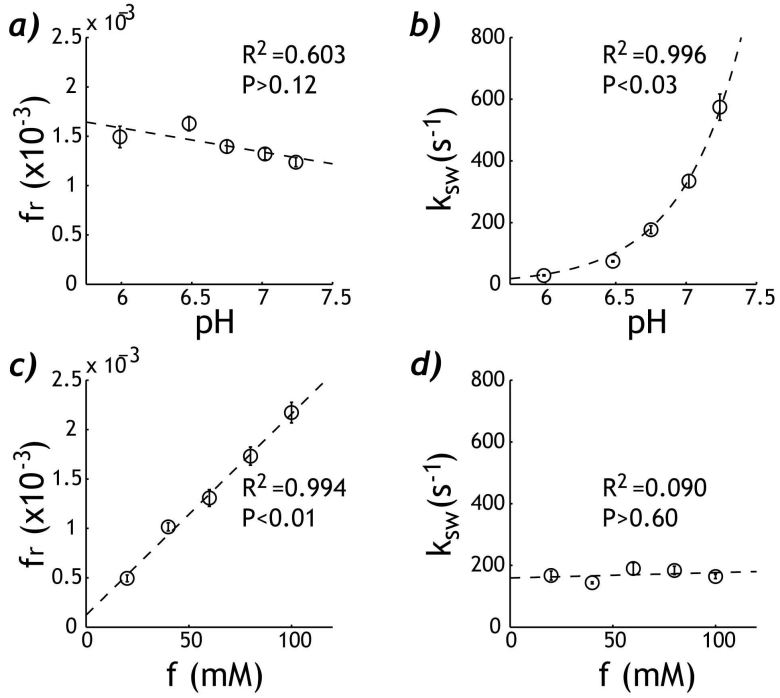

Fig. 5.

Comparison of the derived labile proton ratio and exchange rate. a) For the pH CEST phantom, the labile proton fraction ratio shows little change with pH (R^2=0.603, P>0.12). b) The exchange rate increases exponentially with pH (R^2=0.996, P<0.03). c) For the concentration phantom, the derived labile proton fraction ratio increases linearly with creatine concentration (R^2=0.994, P<0.01). d) The chemical exchange rate shows very little change with the creatine concentration (R^2=0.0903, P>0.60).